EXPERIMENTAL INVESTIGATION OF TRANSONIC FLUID-STRUCTURE INTERACTION PHENOMENA AT A HIGH ASPECT RATIO SWEPT WING

P. C. Steimle,
Aerodynamisches Institut, RWTH Aachen, Wüllnerstraße 5a, 52062 Aachen, Germany

Abstract

An experimental study of transonic flow unsteadiness is presented to characterize three-dimensional shock-boundary layer interaction in the context of aeroelastic instabilities occurring at modern transport type wings. The local interaction between three-dimensional flow and wing structure is analyzed at a high aspect ratio swept wing configuration with supercritical airfoil BAC 3-11/RES/30/21 based on a simplified aeroelastic setup with predefined harmonic wing motion. The structural unsteadiness, which is typically a coupled bending-torsion mode, is separated into the bending and torsional degree of freedom. Wind tunnel experiments have been performed with a variation of the free stream Mach number and angle of attack for low frequency and small amplitude structural oscillations. The focus of the analysis is on two flow cases, one with weak shock-boundary layer interaction with incipient separation and one with strong interaction inducing rear separation.

1. INTRODUCTION

The highly non-linear character of the transonic flow field is a major reason for the occurrence of an unsteady aeroelastic response of the aircraft wing in cruise flight conditions. The unsteady nature of the viscous shock - boundary layer interaction (SBI) induces a time-dependent load distribution on the wing structure. A boundary layer separation induced by the strong pressure gradient generates an unsteady forcing of the wing structure independently from any structural motion, while it affects motion-dependent forces, thereby leading to a negative damping of the aerodynamic field surrounding the wing. The occurrence of dynamic aeroelastic effects is reflected by a sharp decrease of the flutter boundary to a minimum in the high sub-transonic range followed by a rapid recovery close to flight Mach number M_∞ = 1. For a given wing structure the aerodynamic forces increase strongly with the flight speed, while the elastic and inertial forces of the wing structure remain unchanged, resulting in the well-known 'transonic dip' of the flutter boundary [1], [2].

Modern transport aircraft wings with sweep, taper and high aspect ratio typically exhibit a structural response in the first coupled bending – torsion mode. Although the high aspect ratio swept wing is generally receptive to destructive bending – torsion flutter [3], the energy transfer rate from the flow to the wing structure is limited by the aerodynamic non-linearity arising from the shock dynamics to reduce the flutter response to a limit cycle oscillation (LCO) with moderate amplitude. Thus, the non-linearity of the transonic flow not only gives rise to the development of the instability, but also provides a stabilizing attribute that averts the divergent system behavior of classical flutter. Experimental and numerical research activities on the limit cycle phenomenon in the two-dimensional flow regime [4]-[11] come to the conclusion that in general the oscillations are initiated by the unsteady motion of shock waves. This research is aimed at contributing to the efforts on understanding the role of three-dimensional unsteady aerodynamics in transonic flutter. The unsteady aerodynamic field is analyzed on the basis of shock waves of different strengths involving boundary layer separation. To enhance the understanding of the role unsteady three-dimensional flow plays in the transonic fluid-structure interaction, the highly complex system of aero-structural action and reaction is simplified to a predefined harmonic motion of the wing. The focus is on low frequency and small amplitude oscillations of the wing structure, since small surface motion can induce large changes in aerodynamic loading as well as increments in shock excursion relevant at the onset of aeroelastic instabilities.

2. EXPERIMENTAL SETUP

2.1. BAC 3-11 Swept Wing Model

The wind tunnel model under consideration in the experiments is a right side backswept semi-span wing with the supercritical airfoil BAC 3-11/RES/30/21. This airfoil was used in an experimental wind tunnel test campaign in [12]. The thickness to chord ratio is 11%. FIGURE 1 shows the wing model plan form consisting of two segments with a constant leading edge sweep angle of 34° and different trailing edge sweeps of 22° up to a relative half span of η = 0.514 and 26° between 0.514 and the wing tip. With an aspect ratio of 7.54 and taper ratio of 0.38 the wing plan form resembles that of a modern transport aircraft wing. The wind tunnel model is very small with a semi span s = 280mm, and mean aerodynamic chord of $\overline{c}$ = 74.3mm, while the largest chord is 104.35mm at the wing root.

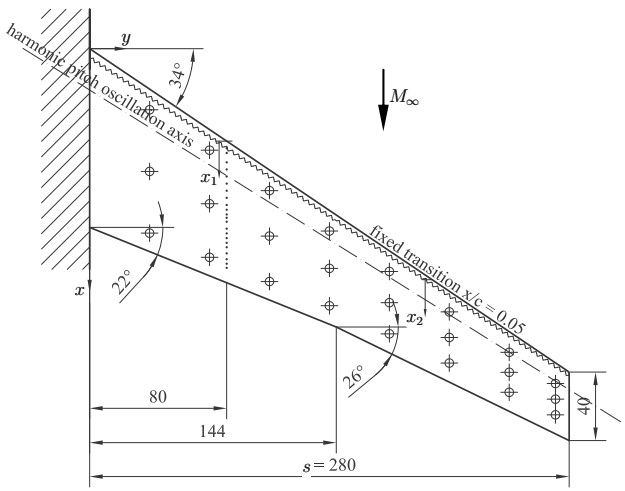

FIGURE 1. Plan view of the supercritical BAC 3-11/RES/30/21 swept wing model, dimensions given in mm.

The wing structure is made of an orthotropic ultra-high modulus carbon fiber laminate sandwich shell. To incorporate measurement equipment into the extremely slender wing structure the sandwich shell is designed as the major structural component without any supporting ribs or spars.

The wing model aeroelastic deformation is measured by videogrammetric tracking of 24 markers distributed in 8 semispan positions on the wing upper surface. The markers have an approximate diameter of 5mm. The wing model is equipped with several subminiature pressure transducers Entran EP-I and Kulite XCQ-080 incorporated in the wing section η = 0.286. The dynamic transducer signals are recorded and digitized with the data acquisition system of the Trisonic wind tunnel at a sample rate of f_s = 20kHz with anti-aliasing filter at 10kHz. Each transducer is installed in closest proximity to the corresponding pressure orifice to minimize the damping and phase shift of the measured pressure signal against the actual signal on the wing surface. As described by Tijdeman in [1], such a connection tube can lead to considerable differences between the true instantaneous pressure and the one measured by the transducer. Following the theory established in [13], the transfer function of the pressure tube connection system incorporated in the composite wing model can be calculated. In the reduced frequency range relevant for the harmonic wing forcing experiments. the damping of pressure fluctuations remains small.

The laminar-turbulent transition of the boundary layer is a significant parameter to determine the shock – boundary layer interaction. To simulate a flow that in most respects resembles a realistic high Reynolds number flow, the boundary layer transition is fixed at a line of 5% chord with a 117µm zic-zac shaped transition strip on the lower side and trip dots of 1mm in diameter and heights between 101.6µm at the wing root and 52.0µm at the tip with a constant spacing of 2mm on the wing upper side. The variable trip dot height is just sufficient to trigger transition to avoid an over fixation of the boundary layer on the upper surface.

2.2. Trisonic Wind Tunnel Facility

The experimental investigation has been conducted in the Trisonic Wind Tunnel of the RWTH Aachen University. This facility is an intermittently working vacuum storage tunnel capable of producing flows with Mach numbers between 0.4 and 3. For transonic flows with freestream Mach numbers below 1, the tunnel is equipped with a 0.4m x 0.4m two-dimensional adaptive test section consisting of parallel side walls and flexible upper and bottom walls to simulate unconfined flow conditions ([14], [15], FIGURE 2). The wall contours are calculated by the one-step method solving the Cauchy integral based on the time-averaged pressure distribution measured along the center line of the flexible walls [16]. The tunnel total pressure and temperature are equal to the ambient conditions. Therefore, the Reynolds number depends on the Mach number and ambient temperature of each test ranging from 1.3 to 1.6 x $10^7 m^{-1}$ in the present experiments. The relative humidity of the airflow is always kept well below 4% at total temperatures around 293K to exclude any influence on the shock wave position [17].

The acoustic environment in the wind tunnel is of major interest in the experimental simulation of dynamic fluid – structure interaction processes. FIGURE 3 displays a summary of frequency spectra measured along the center line of the empty test section for different flow conditions. Depending on the incident Mach number, the acoustic disturbances contain three predominant frequencies, most likely evolving from different acoustic modes in the freestream chamber. The fluctuation power contained in the modes also depends on the Mach number.

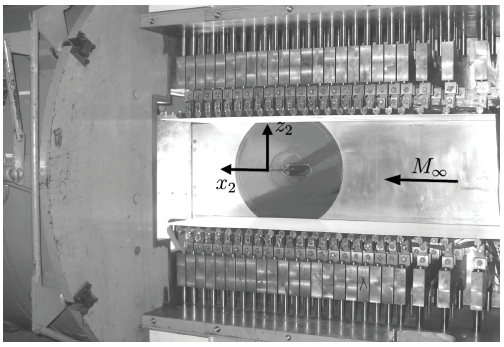

FIGURE 2. Adaptive test section with removed side wall and swept wing model installed.

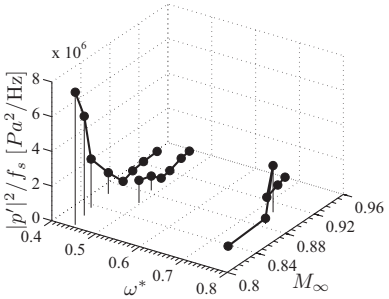

FIGURE 3. Summary of predominant test section frequencies with corresponding fluctuation power over the Mach number for the pressure orifice position closest to the freestream chamber in $[x/c]_2$ = 8.32.

2.3. Anodized Aluminum Pressure-Sensitive Paint Measurements

The unsteady pressure measurement using sensors is limited to one tap section along the half-span of the swept wing model due to geometrical limitations in the wing structure and the small model size in relation to the sensors. Therefore, a coating of pyrene-based pressure sensitive paint (PSP) on porous anodic aluminium binder (AA-PSP), was used to visualize the instantaneous pressure distribution on the upper wing surface with a frequency resolution being high enough to accurately display the dominant events in the dynamic flow. The PSP technique is based on quenching of photo-chemically excited organic molecules by the interaction with oxygen, which allows a measurement of the local oxygen partial pressure by a change in luminescence intensity (FIGURE 4). A complete review can be found e. g. in [18] and [19]. The oxygen permeability of the binder containing the luminophore determines the response time of the PSP luminescence to changes in the local pressure. Very short response times between 35 and 100µs can be realized by using a porous anodic aluminum binder [20], [21], where the photo-chemically active molecule is adsorbed to the pores having direct correspondence with oxygen (FIGURE 5).

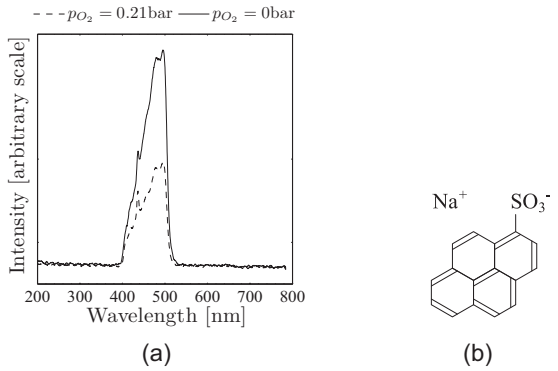

(a) (b)

FIGURE 4. (a) Luminescence intensity spectra of pyrene sulfonic acid on anodized aluminum for different oxygen partial pressures. (b) Chemical composition of 1-pyrene-sulfonic acid sodium salt (PSA), CAS no. 59323-54-5, used as luminophore.

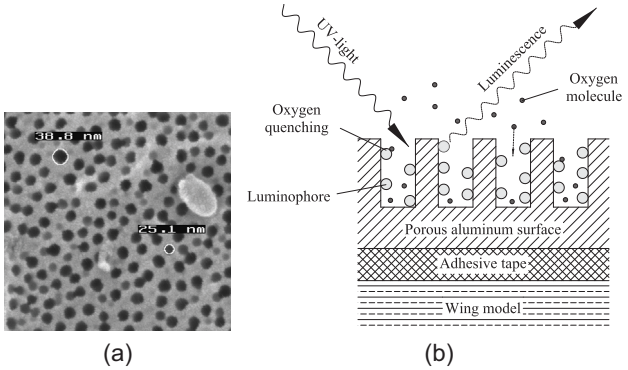

(a) (b)

FIGURE 5. Anodized aluminum pressure-sensitive paint. (a) Scanning electron microscope image of aluminum foil sample anodized with a voltage of 20V, area-related current 15mA/cm^2 at a temperature of 18°C. (b) Schematic representation of the measurement principle.

Similar to a method used in [22] a 47µm aluminum A1050 foil was attached to the carbon fiber wind tunnel model using double sided adhesive tape of 70µm thickness. The model surface was then anodized in 1mol dilute sulphuric acid and covered with pyrene sulfonic acid (PSA) following the procedure of [23]. The pressure-sensitive coating is calibrated using the *a-priori* method. The temperature dependent constants A and B of the Stern-Volmer equation which relates the paint luminescence I to the local absolute pressure P

$$\frac{I_{ref}}{I} = A(T) + B(T)\frac{P}{P_{ref}} \quad (1)$$

are determined for the entire wing surface by applying pressure differences to the model in 'wind-off' condition. The optical setup for the PSP experiments is shown in FIGURE 6. A more detailed description of the calibration method and the optical setup can be found in [24], [25].

The image analysis procedure generally follows [26]. The calculation of the luminescence ratio has to account for the deformation of the wind-tunnel model, which is time-dependent and of large quantity in comparison to other PSP experiments in the literature. The calculation of the intensity ratio used for the local pressure measurement requires a mapping of each measurement image to the reference image. This image registration was performed using the b-spline algorithm described in [27].

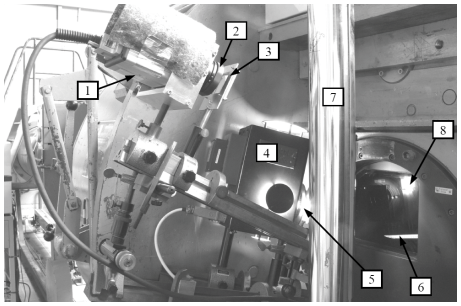

FIGURE 6. AA-PSP visualization setup at the wind tunnel side wall. (1) High-speed CMOS camera, (2) high-aperture objective lens, (3) optical bandpass filter combination, (4) flicker-free UV lamp, (5) bi-convex lens and optical highpass filter, (6) wing model, (7) adjustable stand, (8) test section side window.

3. STEADY WING FLOW PROPERTIES

3.1. Time-Averaged Flow Topology

The unsteady flow involved in aeroelastic interactions in the transonic flight regime is closely linked to the steady flow topology [1]. The steady wing aerodynamics has been investigated for a wide variety of angles of attack and free stream Mach numbers at Reynolds numbers Re_c related to the mean aerodynamic chord $\bar{c}$ around 10^6. The main feature of the transonic swept wing flow is a compression shock terminating the supersonic bubble in the wing flow field. FIGURE 7 displays the Mach number effect on the time-averaged pressure distributions. The supersonic flow area grows with the incident Mach number leading to a stronger shock appearing closer to the trailing edge. Above M_∞ = 0.9 a weak oblique shock is followed by a short supersonic expansion and a strong shock on the

wing upper side. Since the leading shock is caused by a local deflection of the streamlines in the vicinity of the outer boundary layer, the appearance of this shock system marks the change from mild to severe interaction with the boundary layer, which is consistent with the Mach number effect described in [28]-[32]. FIGURE 8 shows the angle of attack effect on the time-averaged pressure distributions for a fixed M_∞ = 0.86. In general, angle of attack and Mach number effect are comparable. The shock wave keeps its time-averaged position at around 62% chord which is a typical behavior attributed to the existence of a separated boundary layer flow.

Anodized aluminum pressure-sensitive paint has been used to measure the time-resolved pressure distribution on the entire upper surface of the swept wing exemplary at $[\alpha_0, M_\infty]$ = [0°,0.86] and [0°,0.92]. At M_∞ = 0.86 the supersonic flow field is still weak, thus extending only to a half-span fraction of about $\eta \approx 0.5$ (FIGURE 9). The shock wave consequently reduces its strength to an isentropic recompression along the half-span. The surface pressure distribution also shows that the overall minimum is located

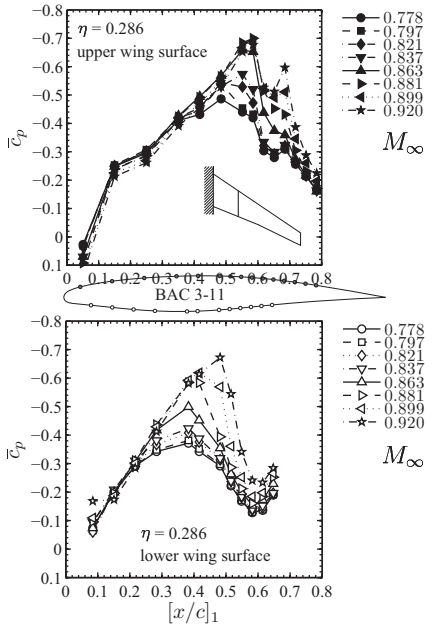

FIGURE 7. Mach number effect on time averaged pressure distributions at η = 0.286 for α_0 = 0°±0.03°.

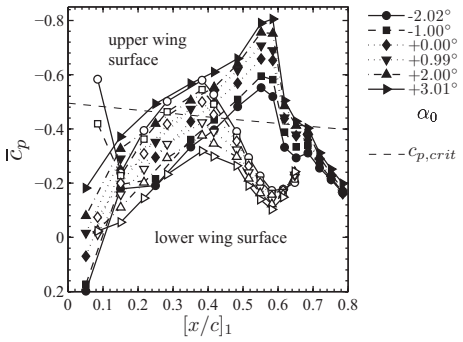

FIGURE 8. Angle of attack effect on time averaged pressure distributions at η = 0.286 for M_∞ = 0.86, Re_c = 1.1x10^6, on the wing upper surface (●, ■, ♦, ▼, ▲, ►, ◄) and lower surface (○, □, ◊, ▽, △, ▷, ◁).

in the region of η = 0.286, where the pressure sensors are located, hence confirming the strategically well positioning of the pressure sensor measurement section. At $[\alpha_0, M_\infty]$ = [0°,0.92] the supersonic field is significantly stronger and extends in the mid-chord region all the way up to the wing tip.

3.2. Definition of Test Cases for the Simulation of Aeroelastic Instabilities

As indicated by the shock stall behavior the wing flow field features a separation of the turbulent boundary layer in the trailing edge region. At low shock strengths, a weak shock – boundary layer interaction with attached flow occurs on the wing upper surface resembling the condition 1 flow described in the Fulker-Ashill model [33]. The flow exhibits a pronounced cross flow component and separates close to the trailing edge (FIGURE 10a). Nevertheless, a shock-induced separation developing out of a marginally separated flow in the shock foot region due to intense skewing of the velocity profile and the trailing edge separation is incipient at $[\alpha_0, M_\infty]$ = [0°,0.86]. A further increase in the shock strength results in a separation at the shock foot merging with the trailing edge separation, which is also associated with the first lift divergence. The appearance of the lambda shock system at higher Mach numbers 0.9 and 0.92 corresponds with a full scale separation from the

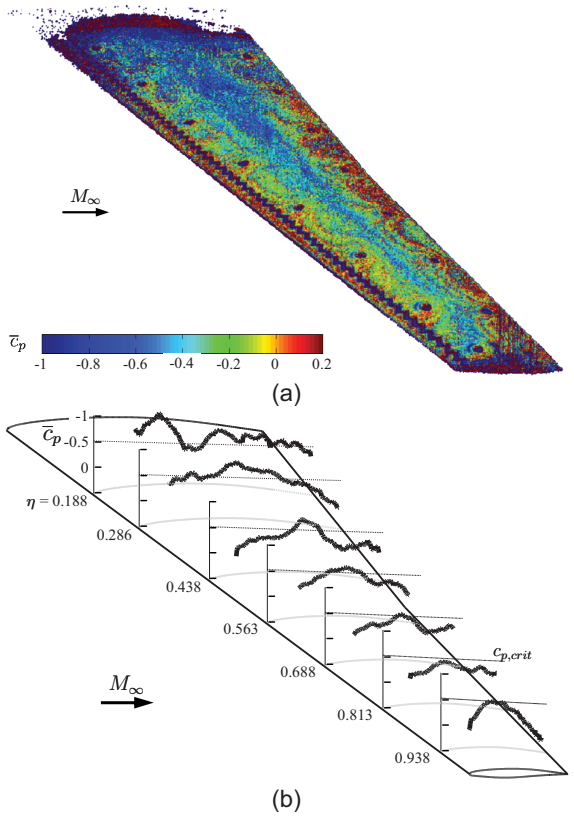

FIGURE 9. Time-averaged pressure distribution on the upper wing surface measured with AA-PSP and isothermal a-priori calibration, α_0 = 0°, M_∞ = 0.86, image acquisition rate f_s = 1500Hz, 3000 samples used for averaging. (a) Color-coded representation of the three-dimensional pressure distribution. (b) Section-wise extraction along the half-span in η = 0.188, 0.286, 0.438, 0.563, 0.688, 0.813, and 0.938.

shock foot to the trailing edge involving a secondary boundary layer flow in the direction of the cross-wise pressure gradient (FIGURE 10b). The change from condition 2 in the Fulker-Ashill flow model with a slight separation bubble to condition 3 with fully separated trailing edge flow is hard to detect with the oil flow technique, since it is a very rapid process of arbitrary character.

Force measurements at the fixed BAC 3-11 wing show a lift and drag divergence Mach number around M_∞ = 0.86 for α_0 = 0°. The divergence of aerodynamic derivatives is known to coincide with the first occurrence of aeroelastic instabilities in the vicinity of the flutter stability minimum observed in the sub-transonic speed regime. Schewe *et al.* [34] conclude their analysis of flutter tests conducted with a supercritical airfoil that flow separation and its interaction with the shock wave most likely cause the aeroelastic instability limit to increase towards higher Mach numbers and that, therefore, the transonic dip minimum is observed to occur close to the lift-divergence Mach number. Although flutter characteristics cannot be determined in the Trisonic Wind Tunnel facility, the single shock wave flow at $[\alpha_0, M_\infty]$ = [0°,0.86] is suspected to be close to the minimum of the stability boundary curve, commonly referred to as “transonic dip” [1], while the lambda shock flow with full scale trailing edge separation at $[\alpha_0, M_\infty]$ = [0°,0.92] is on the increasing branch of the stability limit. In the following analysis of transonic flow unsteadiness, these two flows are used as test cases for the unsteady wing experiments.

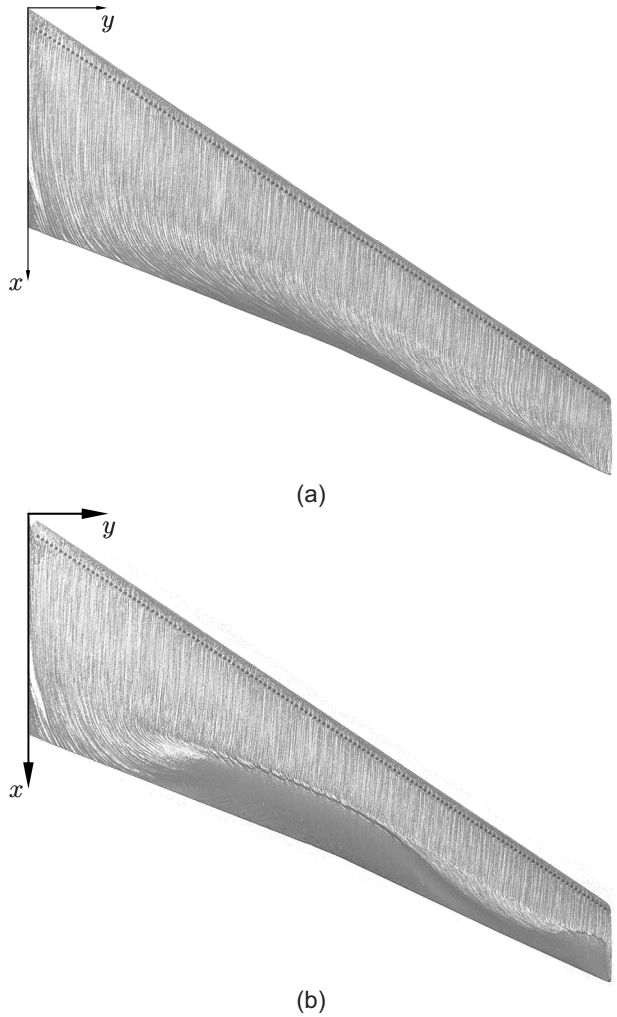

FIGURE 10. Surface flow pattern on the wing upper surface. The significant deflection of the skin friction lines is caused by a strong chordwise pressure gradient which induces separation near the trailing edge. (a) α_0 = -0.02°, M_∞ = 0.859, shock strength not sufficient to separate the boundary layer. (b) α_0 = 0.02°, M_∞ = 0.921, shock induced separation.

3.3. Transonic Flow Field Unsteadiness

In FIGURE 11 the pressure distribution in η = 0.286 is plotted against the stream-wise co-ordinate including the minima and maxima of the respective pressure coefficients denoted by error bars. It is quite obvious that this flow is a very unsteady one, even in the absence of forced structural motions with the shock wave being the major source of this behavior. In the region of the time-averaged shock position and interaction with the boundary layer downstream the largest pressure fluctuations occur. The spectral analysis of the wing flow unsteadiness reveals several reduced frequencies $\omega^* = 2\pi f \bar{c}/u_\infty$ incorporated in the flow dynamics of the weak shock test case. The fluctuation of the shock properties on the upper surface (FIGURE 11c - f) essentially contains the reduced frequencies ω^* = 0.43 including its first harmonic, and 0.73. In this analysis the shock deflection angle β and shock angle θ are calculated from the time-dependent pressure distribution using the oblique shock relationships and the Rankine-Hugoniot equations taking into account the local oblique shock sweep angle determined by a close-up analysis of the oil flow visualization following [35] and [36].

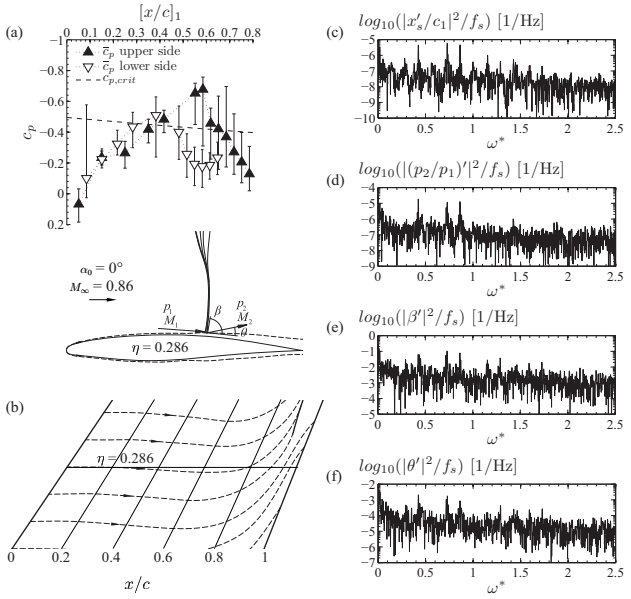

FIGURE 11. Overview of the weak shock test case, α_0 = 0.02°, M_∞ = 0.861, Re_c = 1.08x10^6, wing upper surface, η = 0.286. (a) Time-averaged pressure distribution. (b) Skin friction lines in the area of η = 0.286 visualized with the oil flow technique. (c) Power spectrum of fluctuations in the shock position x_s/c_1. (d) Power spectrum of fluctuations in the shock strength p_2/p_1. (e) Power spectrum of fluctuations in the shock angle β. (f) Power spectrum of fluctuations in the deflection angle θ.

This type of periodic flow unsteadiness is strongly present in the range of α_0 = 0°, M_∞ = 0.84 to 0.88 and changes to a different kind of unsteadiness at M_∞ = 0.90 and 0.92. Since the time-averaged shock foot position shifts downstream at rising Mach number, it coincides with the trailing edge separation line thereby replacing the dynamic interaction between shock foot and the cross-flow with a rather steady separation line resulting in a rather steady position of the leading oblique shock branch (FIGURE 12). This characteristic is a result of the cross-flow in the separated region which is not subject to major disturbances from the inviscid flow above. The downstream shock on the other hand exhibits strong fluctuations with the fluctuation power solely contained in ω^* = 0.72. The local deflection angle shows a more pronounced fluctuation (FIGURE 12f) due to the pulsation of the separated boundary layer, in comparison to the weak shock flow.

The onset of periodic shock oscillations was investigated in several experimental and numerical flow analyses. Brunet et al. describe a “pulsation” of the separated area to be the origin of buffet oscillations on the OAT15A supercritical airfoil with a thickness to chord ratio of 12.5% [37]. Lee’s widely accepted acoustic feed-back model [38] describes the inviscid shock interaction with upstream propagating sound waves generated by the impingement of large scale turbulent eddies on the sharp trailing edge [39] forming a feedback loop with disturbances convected downstream to be the main buffet mechanism. Shock buffet has mainly been investigated in two-dimensional flows [7], [38], [40]. The observed reduced buffet frequency of ω^* = 0.73 on the BAC 3-11 wing is in the range of that of other supercritical airfoils with this thickness ratio and comparable shock position.

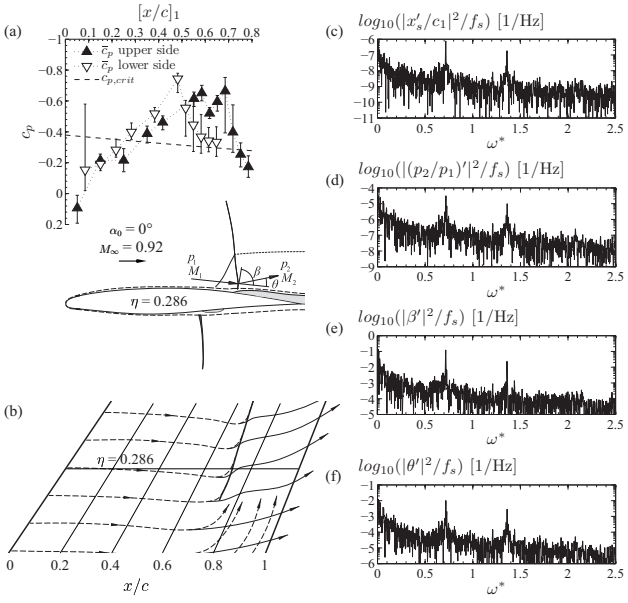

FIGURE 12. Overview of the strong shock test case, α_0 = 0.02°, M_∞ = 0.919, Re_c = 1.11x10^6, wing upper surface, η = 0.286. (a) Time-averaged pressure distribution. (b) Skin friction lines in the area of η = 0.286 visualized with the oil flow technique. (c) Power spectrum of fluctuations in the shock position x_s/c_1. (d) Power spectrum of fluctuations in the shock strength p_2/p_1. (e) Power spectrum of fluctuations in the shock angle β. (f) Power spectrum of fluctuations in the deflection angle θ.

Nevertheless, the shock buffet phenomenon observed on the BAC 3-11 swept wing has a different characteristic than shock buffet flows described in the literature. In the case of classical buffet the shock is strong enough to cause a fully separated flow between the shock boundary-layer interaction area and the trailing edge. The formation of the acoustic feed back loop can be observed at high Mach numbers and high angles of attack. In the BAC 3-11 three-dimensional buffet flow considered here, the cross-flow region with skewed boundary layer profile is unsteady and leads to an oscillatory shock motion due to the local interference in the shock foot. The presence of the separated flow activates the trailing edge as sound source to induce acoustic waves to the shock even at low angles of attack.

4. HARMONIC FORCING EXPERIMENTS

The unsteady motion of a high aspect ratio swept is modeled by a two-degree-of-freedom aeroelastic system with the bending and torsional degree of freedom (FIGURE 13). Experiments have been conducted to simulate unsteady fluid-structure interaction by a simplified aeroelastic setup in either the bending degree of freedom by heave oscillations $h(t) = h_1 \sin(\omega_h\, t)$ or the torsional degree of freedom by pitch oscillations $\alpha(t) = \alpha_0 + \alpha_1 \sin(\omega_\alpha\, t)$. The harmonic structural oscillation with controllable amplitude and frequency can be used to investigate the sensitivity of unsteady aerodynamic processes observed in the swept wing flow to structural unsteadiness, thereby providing a further insight into the development of aeroelastic instabilities in this highly complex flow.

A special feature of the forced oscillation experiments is the harmonic wing motion with several relatively low fundamental frequencies $\omega^* \leq 0.125$ in the presence of self-induced shock oscillations, due to an aero-acoustic feedback with trailing edge noise. Regarding the interaction between the shock buffet and the oscillating wing structure, a general effect of the forced harmonic wing oscillation can be observed in the frequency spectra of wing surface pressure fluctuations. The influence of the test section resonance reduces significantly at ω^* = 0.425 and 0.865, while the shock buffet at ω^* = 0.73 starts to dominate the field (FIGURE 14). Obviously, the structural motion causes a coupling into the buffet frequency due to the trailing edge oscillation probably causing an amplification in the noise producing mechanism.

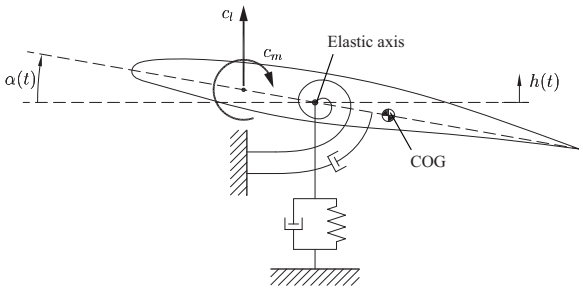

FIGURE 13. Idealized two-degree-of-freedom aeroelastic system.

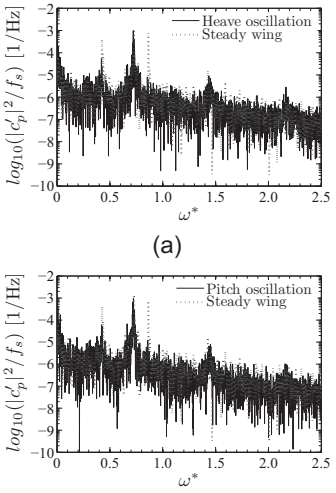

FIGURE 14. Frequency coupling in the pressure fluctuation power spectra of the SBI region, η = 0.286, weak SBI flow. (a) Harmonic heave oscillations with h_1/s = 0.086%, ω_h^* = 0.026. (b) Harmonic pitch oscillations with α_1 = 0.155°, ω_α^* = 0.025.

4.1. First Harmonic Pressure Distributions

The aerodynamic response function to harmonic oscillations of the wing structure can be assessed using the first harmonic unsteady pressure distribution calculated with the Fourier coefficients of the pressure fluctuation $C_p(\mathrm{i}\omega)$ and the heave motion $H(i\omega)$ or pitch motion $\alpha(i\omega)$ at the fundamental frequency $\omega_{h\,\dot{\vee}\,\alpha}$.

$$(2)\quad H_{c_p,\,h} = \frac{C_p(\mathrm{i}\omega_h)}{H(\mathrm{i}\omega_h)},\; H_{c_p,\,\alpha} = \frac{C_p(\mathrm{i}\omega_\alpha)}{\alpha(\mathrm{i}\omega_\alpha)}$$

Hence, the harmonic variation of the pressure distribution can be described by the magnitude $|H|$ and phase $\varphi(H)$ related to the local wing section motion (FIGURE 15, FIGURE 16). Despite the limited influence a pure vertical wing motion can have directly on the transonic flow field via the induced angle of attack, both flow test cases seem to very sensitive to pure heave motions, especially in the SBI region and especially at smallest amplitudes and frequencies due to the pronounced sensitivity of strong shock waves to low frequency perturbations in general [41]. The local shock unsteadiness which is induced by Kutta waves originating from the trailing edge is amplified by the slight motion of the trailing edge in the separated flow and wake thickness order of magnitude. It is thereby demonstrated that the low frequency – low amplitude heave motion has the potential to destabilize the wing structure, although with beneficial character, since the flow response always reduces with higher amplitudes. This observation complies with the general statement that small disturbances can have large effects in the unsteady transonic flow field.

The unsteady harmonic pressure distributions furthermore show the subtle stability of the dynamic shock – boundary layer interaction against the influence of the harmonic pitch motion of the wing section. This intrinsic stability arises from the shock motion, which is induced by the acoustic feed-back in the rear part of the airfoil. Presumably, the characteristic of the sound source in the trailing edge does not change with the pitch motion, since the trailing edge motion is of much larger quantity than the length scales in the shear flow interaction with the trailing edge. Concerning the dynamic shock – boundary layer interaction this is probably the most important difference to the effect of the harmonic heave motion.

The comparison of the unsteady pressure distributions of the weak and strong SBI flow demonstrates an important effect buffet has on harmonic wing oscillations. Compared to the unsteady weak shock flow case the lambda shock flow is much more sensitive to disturbances from the wing structure and exhibits a rather strong harmonic oscillation with the fundamental frequency (FIGURE 16). The effect is most significant at very small pitch oscillations. Obviously, the shock buffet mechanism in the weak shock flow case has a stabilizing influence on the fluid – structure interaction, since the wing oscillation cannot change the acoustic feedback loop being the origin of the buffet oscillation. On the other hand, the lambda shock pattern quickly adjusts to changes in the local boundary layer, especially to the position of the trailing edge separation line, which depends on the instantaneous local angle of attack.

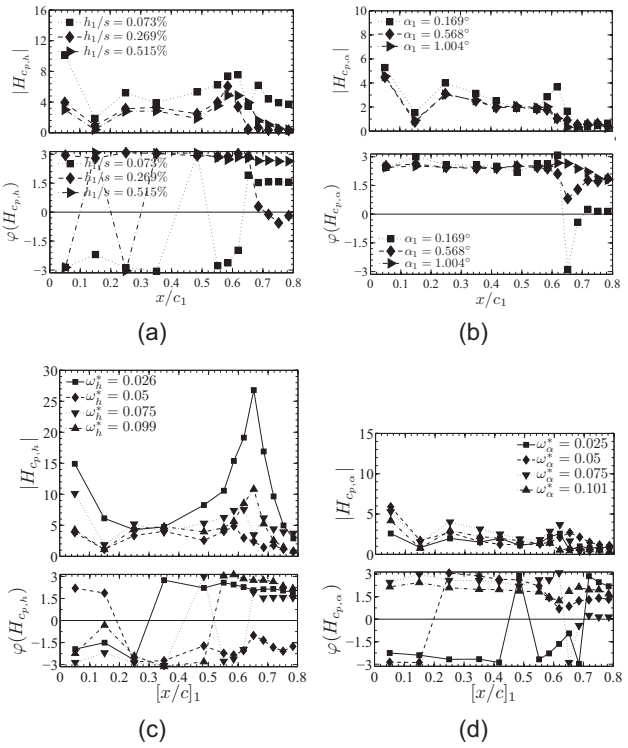

FIGURE 15. 1st harmonic pressure distribution in η = 0.286 on the upper surface for weak SBI flow. (a) Heave amplitude effect at ω_h^* = 0.075. (b) Pitch amplitude effect at ω_α^* = 0.075. (c) Heave frequency effect at 0.073% ≤ h_1/s ≤ 0.136%. (d) Pitch frequency effect at 0.154°≤ α_1 ≤ 0.168°.

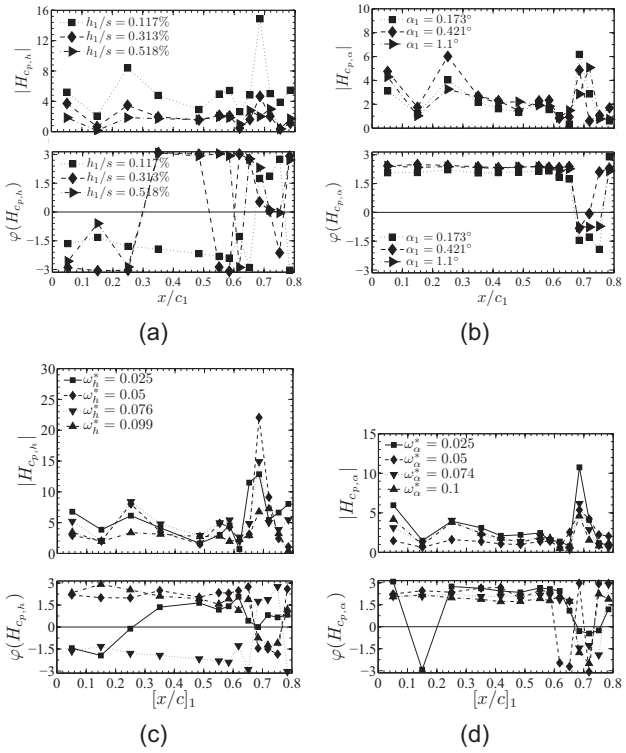

FIGURE 16. 1st harmonic pressure distribution in η = 0.286 on the upper surface for strong SBI flow. (a) Heave amplitude effect at ω_h^* = 0.075. (b) Pitch amplitude effect at ω_α^* = 0.075. (c) Heave frequency effect at 0.077%≤ h_1/s ≤ 0.136%. (d) Pitch frequency effect at 0.121°≤ α_1 ≤ 0.179°.

4.2. Local Fluid-Structure Energy Exchange

The probably most important aspect in the analysis of the dynamic pressure distribution is the energy exchange between the transonic flow field and the wing structure, since it determines the development of aeroelastic instabilities potentially occurring in cruise flight condition. The averaged local energy exchange on the unsteady wing can be estimated based on the method proposed by Dietz *et al.* [42]. The local energy exchange in the different flow cases is examined based on the time-resolved pressure distribution in η = 0.286 combined with the synchronous measurement of the wing motion in the heave and pitch degree of freedom at the same location (FIGURE 17).

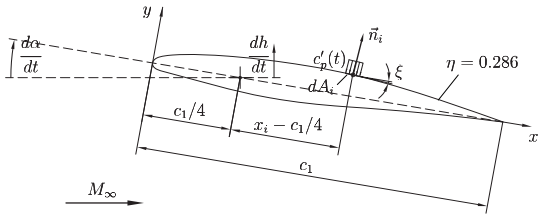

FIGURE 17. Determination of the local work coefficient at the stream-wise swept wing section.

If the skin-friction contribution to the energy exchange is neglected, the fluid-structure energy exchange can be calculated by the time-dependent motion of the exchange boundary and the pressure fluctuation acting on it. The local work coefficient $\bar{c}_w$ describes the local work exerted by the pressure fluctuating quantity c_p' on a surface element dA_i with the corresponding normal vector $\vec{n}_i$ and instantaneous local velocity $\vec{v}$ of the wing surface in the chord-wise position x_i/c_1 in one harmonic wing oscillation period T.

$$c_w(x_i/c_1) = \frac{1}{dA_i} \int_{t-T/2}^{t+T/2} -c_p'(x_i/c_1, t)\, \vec{n}_i\, dA_i\, \vec{v}(x_i/c_1, t)\, dt \quad (3)$$

This methodology can of course only be applied to locations on the wing surface, where the instantaneous pressure distribution is a known quantity. Since the result from the PSP measurements contain a significant amount of optical noise, only the pressure distribution at η = 0.286 is used in this analysis. However, in principle it is possible to extrapolate the local analysis to the entire wing surface based on the observation in the PSP measurements that pressure fluctuations on the surface develop similarly along the wing span with a decrease in shock strength.

The occurrence of a weak shock wave, which develops along with a decrease of the aeroelastic stability boundary towards the transonic dip minimum, amplifies the excitatory effect of the fluid-structure interaction to promote a dynamic response of the wing. In the weak shock flow the SBI region is the source of a strong energy production, although the shock oscillation yields much higher frequencies than the harmonic wing motion due to the shock buffet. FIGURE 18 shows a pronounced amount of work performed locally on the structure, especially in the time-averaged shock position around $[\bar{x}_s/c]_1$ = 0.62. The cross-flow region in the rear of the wing section in η = 0.286 on the other hand exhibits negative values of the mean work coefficient illustrating the damping nature of the boundary layer flow with skewed velocity profile.

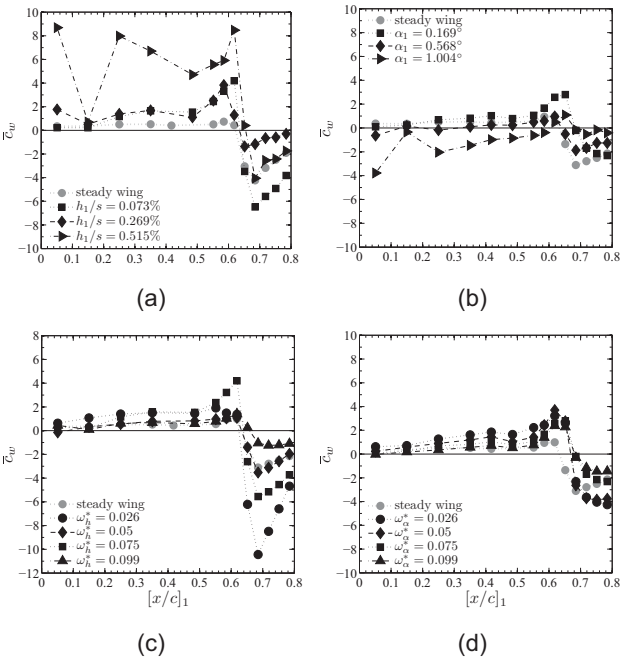

FIGURE 18. Time-averaged work coefficient in η = 0.286 on the wing upper surface for the weak SBI flow, forced heave oscillation. (a) Heave amplitude effect for ω_h^* = 0.075. (b) Pitch amplitude effect at ω_α^* = 0.075. (c) Heave frequency effect for 0.073% ≤ h_1/s ≤ 0.136%. (d) Pitch frequency effect for 0.154° ≤ α_1 ≤ 0.168°.

The work coefficient grows progressively with the heave amplitude (FIGURE 18a, c), especially at ω_h^* = 0.075, while at other fundamental frequencies the damping effect of the cross-flow region compensates the excitation in the shock foot. The special sensitivity to this particular reduced frequency is attributed to the interference with the shock buffet, since the fundamental frequency is close to a multiple of the buffet frequency, thus feeds fluctuation power into the flow oscillation In case of harmonic heave oscillations the damping arises solely from the pronounced cross-flow, although the existence of a dynamically developing separated flow cannot be excluded. The heave amplitude effect would have the general potential to drive a destructive flutter amplitude increase, if pure bending motion were the main structural unsteadiness. When the pitch DOF is activated and heave response suppressed, the energy exchange is reduced (FIGURE 18b, d). The excitation from the supersonic flow region even turns into a neutral or damping behavior at higher amplitudes as well as frequencies.

The amplitude effect in the case of wing pitching motion demonstrates the self-regulating mechanism in the aeroelastic system for the weak shock flow case, which is near the minimum of the transonic dip in the aeroelastic stability curve. In this flow case wing unsteadiness may develop into a limit cycle oscillation, if the pitching degree of freedom is primarily involved. This conclusion is consistent with the analysis of swept wing transonic limit cycle flutter given by Bendiksen [43], [44] attributing the positive influence of the bending-torsion coupling and structural washout on the limitation of flutter amplitudes.

In the strong SBI flow (FIGURE 19) the fluctuations are generally much weaker yielding a lower level of energy exchange between flow and structure. The pronounced excitatory effect of the supersonic flow region, however, is comparable to the weak SBI flow. This excitation is also accompanied by a damping in the separated flow in closest proximity to the lambda shock pattern. This flow characteristic supports the proposition of Tichy [45] that the development of separated flow is responsible for the increase of the aeroelastic stability limit at higher M_∞. The damping effect cannot be attributed merely to the existence of the separation, but primarily to the local shock wave interaction with the separated flow.

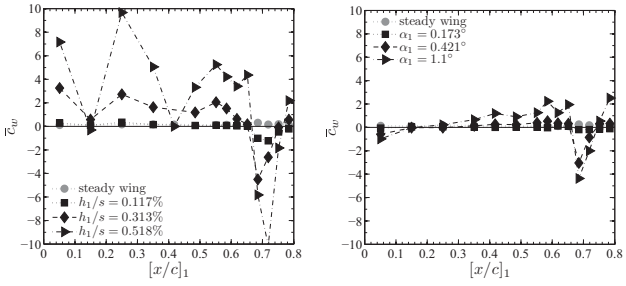

(a) (b)

FIGURE 19. Time-averaged work coefficient in η = 0.286 on the wing upper surface for the strong SBI flow. (a) Heave amplitude effect for ω_h^* = 0.075. (b) Pitch amplitude effect at ω_α^* = 0.075.

In the separated flow region a different behavior can be observed. Unlike the cross-flow region in the weak SBI flow, the full-scale trailing edge separation exhibits an excitation of the wing structure in a certain distance to the lambda shock pattern. The pulsation of the rear separation is obviously also able to excite the structure under these circumstances. This observation is in qualitatively good agreement with the energy exchange described for the NLR 7301 profile as test case TL4 by Dietz *et al.* in [42]. This situation is aggravated by the progressively increasing excitation in the supersonic flow developing in pitch oscillations with increasing amplitude. Here, also the lower shock with induced separation and reattachment contributes to the structural excitation at higher pitch amplitudes. Hence, from the viewpoint of this analysis the lambda shock flow has the potential to initiate a strong flutter response of the wing. Amplitude limiting effects cannot be detected in the investigated oscillation parameter range. The arising structural excitation in the supersonic flow field at large pitching amplitudes can be attributed to a lack of intrinsic stability, which is present in the weak shock flow case due to the pronounced shock buffet at ω^* = 0.72. Nevertheless, destructive wing flutter might be avoided at higher amplitudes by another bifurcation in the flow behavior with the shock motion on the wing upper surface itself absorbing more energy from the structural oscillation.

5. CONCLUSION

While the presence of an aero-acoustic mechanism induces shock buffet, the shock wave is demonstrated to behave rather differently depending on its strength and the resulting nature of the boundary layer flow. At the weak shock wave the boundary layer flow is deflected towards the tip, thereby probably developing a marginally separated flow. The shock foot region exhibits strong fluctuations, constituting an environment of strong dynamic loads, but also causing an inherent dynamic stability of the SBI region against other disturbances, as demonstrated by harmonic forcing of the wing model. At increased shock strength, the full-scale separation from the shock foot to the trailing edge induces a noticeable decrease of pressure fluctuations induced to the surface. Next to the presence of an additional layer in the flow near the boundary, this locally reduced flow dynamic also arises from the steady nature of the separation line, due to the transversal flow and the asymptotical progression of the surface stream lines into the separation line. Nevertheless, an excitation of the wing structure can arise from the pulsation of the separation. At strong SBI, it can be concluded that it is not the presence of the separated flow leading to a damping of the surface fluctuations, but the SBI itself. The localized shock oscillation not only derives its oscillatory power from aero-acoustic disturbances, but also from pressure fluctuations in the SBI region. While the forced harmonic pitch motion of the wing structure generates an unsteady flow response reducing at higher structural amplitudes, the pure bending motion shows the possible development of destructive flutter. This result, however, is merely of theoretical nature, since the bending – torsion coupling of swept wings always provides some pitching response for the wing motion to enter a beneficial limit cycle. But it is certainly the main contribution of the bending to aeroelastic instabilities to trigger the first initiation of

the structural unsteadiness.

The current experiments have demonstrated the potentially harmful effect of structural oscillations in the pure bending degree of freedom. This particular aspect might have a further relevance to future composite wing designs with adjustable stiffness distribution. The directional material characteristics could be selected appropriately to specifically counteract the initiation of transonic flutter, thereby reducing the necessary flutter margin in future transport aircraft designs.

This research is funded by the Deutsche Forschungsgemeinschaft within the Collaborative Research Center SFB 401 “Flow Modulation and Fluid-Structure Interaction at Airplane Wings”.

6. REFERENCES

[1] Tijdeman, H. (1977) Investigation on the Transonic Flow around Oscillating Airfoils. PhD thesis, NLR TR 77090 U, TU Delft, The Netherlands.
[2] Tijdeman, H., Seebass, R. (1980) *Ann. Rev. Fluid Mech.* **12** 181-222.
[3] Bendiksen, O. O. (2001) *J. Guidance, Control, and Dynamics* **24** (1) 176-184.
[4] Kousen, A., Bendiksen, O. O. (1994) *J. Aircraft* **31** (6) 1257-63.
[5] Bendiksen, O. O. (1992) Role of Shock Dynamics in Transonic Flutter. AIAA-Paper 92-2121.
[6] Schewe, G., Deyhle, H. (1996) Experiments on transonic flutter of a two-dimensional supercritical wing with emphasis on the non-linear effects. Royal Aeronautical Society Conference on Unsteady Aerodynamics, July 17-18 1996, London, UK.
[7] Schewe, G., Knipfer, A., Mai, H., Dietz, G. (2002) Deutsches Zentrum für Luft- und Raumfahrt internal report DLR-IB 232-2002 J 01.
[8] Schewe, G., Mai, H., Dietz, G. (2003) *J. Fluids Structures* **18** 3-22.
[9] Geissler, W. (2003) *Aerosp. Sci. Technol*. **7** (77) 540-550.
[10] Bendiksen, O. O. (2004) AIAA-Paper 2004-1694.
[11] Dietz, G., Schewe, G., Mai, H. (2006) *J. Fluids Structures* **22** 505-527.
[12] Moir, I. R. M. (1994) Measurements on a two-dimensional aerofoil with high-lift devices. AGARD Advisory Report 303, DRA, Farnborough, United Kingdom.
[13] Bergh, H., Tijdeman, H. (1965) Theoretical and experimental results for the dynamic response of pressure measuring systems. NLR Technical Report F.238.
[14] Romberg, H.-J. (1990) *J. Aircraft* **38** (4) 177-180.
[15] Wolf, S. W. D. (1995) *Prog. Aerospace Sci.* **31** 85-136.
[16] Amecke, J. (1985) Direkte Berechnung von Wandinterferenzen und Wandadaption bei zweidimensionaler Strömung in Windkanälen mit geschlossenen Wänden (in German). DFVLR-FB 85-62.
[17] Binion, T. W. (1988) AGARDograph 303, sec. 4.
[18] Bell, J. H., Schairer, E. T., Hand, L. A., Mehta, R. D. (2001) *Ann. Rev. Fluid Mech.* **33** 155-206.
[19] Klein, C. (2000) *Aerosp. Sci. Technol*. **4** 103-109.
[20] Sakaue, H., Sullivan, P. (2001) *AIAA J.* **39** (10) 1944-1949.
[21] Sakaue, H., Gregory, J. W., Sullivan, J. P. (2002) *AIAA J.* **40** (6) 1094-1098.
[22] Mérienne, M.-C., Le Sant, Y., Ancelle, J., Soulevant, D. (2004) *Meas. Sci. Technol.* **15** 2349-2360.
[23] Kameda, M., Tezuka, N., Hangai, T., Asai, K., Nakakita, K., Amao, Y. (2004) *Meas. Sci. Technol*. **15** 489-500.
[24] Steimle, P. C., Karhoff, D.-C., Nakata, S., Schröder, W. (2009) Unsteady Anodized Aluminum Pressure-Sensitive Paint Measurements on a High Aspect Ratio Swept Wing in Transonic Flow. AIAA Intl. Forum on Aeroelasticity and Structural Dynamics, 22 – 25 June 2009, Seattle, WA, USA, Paper No. IFASD-2009-122.
[25] Steimle, P. C. (2009) Experimental Investigation of Transonic Fluid-Structure Interaction Phenomena at a High Aspect Ratio Swept Wing. Doctoral thesis D82, RWTH Aachen University, Shaker, Aachen, Germany.
[26] Asai, K., Kanda, H., Cunningham, C. T., Erausquin, R., Sullivan, J. P. (1997) Surface pressure measurements in a cryogenic wind tunnel by using luminescent coatings. 17th Int. Congr. Instrumentation in Aerospace Simulation Facilities (ICIASF), 28 Sept. – 2 Oct 1997.
[27] Rueckert, D., Sonda, L. I., Hayes, C., Hill, D. L. G., Leach, M. O., Hawkes, D. J. (1999) *IEEE Transactions on Medical Images* **18** (8) 712-721.
[28] Seddon, J. (1960) RAE TM Aero 667, R&M 3502.
[29] Green, J. E. (1971) AGARD Conference Proceedings 81, 2-1 – 2-12.
[30] Adamson, T. C. Jr., Messiter, A. F. (1980) *Ann. Rev. Fluid Mech.* **12** 103-138.
[31] Délery, J. M. (1985) *Progr. Aerosp. Sci*. **22** 209-280.
[32] Délery, J., Marvin, J. G. (1986) Shock-Wave Boundary Layer Interactions. AGARDograph 280 90-108.
[33] Fulker, J. L., Ashill, P. R. (1986) A Model of the Flow over Swept Wings with Shock Induced Separation. In: Délery, J. (Ed.) Turbulent Shear Layer / Shock Wave Interactions, IUTAM Symposium Palaiseau 1985, Springer, Berlin, Heidelberg, Germany.
[34] Schewe, G., Mai, H., Dietz, G. (2003) *J. Fluids Structures* **18** 3-22.
[35] Inger, G. R. (1984) AIAA-Paper 1984-1555.
[36] Stanewsky, E. (1988) AGARD Advisory Report 224, 271-305.
[37] Brunet, V., Deck, S., Jacquin, L., Molton, P. (2006) Transonic Buffet Investigations Using Experimental and DES Techniques. 7th ONERA-DLR Aerospace Symposium ODAS 2006, Toulouse, France. ONERA-TP-2006-165.
[38] Lee, B. H. K. (2001) *Progr. Aerosp. Sci*. **37** 147-196.
[39] Deck, S. (2005) *AIAA J*. **43** (7) 1556-1566.
[40] Finke, K. (1977) Stoßschwingungen in schallnahen Strömungen (in German). VDI-Forschungsheft 580, VDI-Verlag, Düsseldorf, Germany.
[41] Dussauge, J-P., Piponniau, S. (2008) *J. Fluids Structures* **24** 1166-1175.
[42] Dietz, G., Schewe, G., Mai, H. (2006) *J. Fluids Structures* **22** 505-527.
[43] Bendiksen, O. O. (2007) Effect of Wing Deformations and Sweep on Transonic Limit Cycle Flutter of Flexible Wings. AIAA/CEAS/KTH Int. Forum on Aeroelasticity and Structural Dynamics, Stockholm, Sweden.
[44] Bendiksen, O. O. (2008) *J. Aircraft* **45** (5) 1522-1533.
[45] Tichy, L. (1992) Transsonische Strömungen an einem schwingenden Profil und deren Einfluß auf die Flattergrenze. Dissertation, Technische Universität München, DLR Fachbericht 92-08 (in German).